Nonlinear Hyperlens

Daniel Aronovich and Guy Bartal*

Department of Electrical Engineering, Technion–Israel Institute of Technology, Haifa 32000, Israel
**Corresponding author:* guy@ee.technion.ac.il

The performance of the optical Hyperlens, made of metal-dielectric layers, can be improved by incorporating self-focusing nonlinearity in the dielectric layers. Using home-developed modified Beam Propagation Method in cylindrical coordinates we show increased bandwidth and better propagation length which can improve the spatial and temporal resolution of the device.

Optical Hyperlens [1–5] was studied extensively in the past few years owing to its capability of conveying Subwavelength information into the far field while overcoming the diffraction limit [6], thereby showing great promise in real-time nanoscale optical imaging and sensing. The unique formation of the hyperlens, made of alternating nanolayers of metal and dielectric with period much smaller than the wavelength of the light, gives rise to a strong form birefringence which can result in opposite signs of the electrical permittivity along different axes, yielding hyperbolic dispersion relations [7]. This property , on top of enabling negative refraction [8–10], also allows Subwavelength imaging by removing the high spatial frequencies cutoff as exists in free space. Concurrently, the curved geometry adiabatically enlarges the small features, converting evanescent to propagating waves.

Imaging by Hyperlens is achievable when the electrical permittivity along the axis perpendicular to the propagation direction approaches zero, eliminating all diffraction effects [2,11]. This condition is termed the "cancelation regime" or "perfect imaging" and requires working conditions close to the SPP resonance in the structure, where the magnitudes of the dielectric constants of the metal and the insulator become comparable [12,13]. This constraint limits the device operation as, close to resonance, one encounters high losses. Namely, an inherent trade-off between diffraction and loss is imposed. Furthermore, the sensitivity to frequency changes close to the resonance results in limited bandwidth.

The performance of the hyperlens can be vastly improved by relaxing the SPP resonance condition and finding alternative ways to suppress the resultant diffraction. A promising direction is by utilizing self-focusing nonlinearity, e.g., using dielectric layers with high Kerr-type nonlinearity. The nonlinearity induces a local change in the electrical permittivity which is proportional to the intensity pattern, which in turn, can alter the diffraction in the structure. This approach have already shown to support subwavelength solitons in metal-dielectric nanolyares [14]. In this work, we present a nonlinear hyperlens made of alternating layers of metal and nonlinear dielectric. We show that by introducing nonlinearity the diffraction is suppressed and the operation frequency range of the device can be extended where longer propagation distance can be achieved. The sub-wavelength propagation in such nonlinear hyperbolic medium is simulated using a self-developed nonlinear beam propagation method (NL-BPM) in cylindrical coordinates that is applicable for any non-paraxial propagation along the *radial* direction.

To convey the main concept, we start by introducing a simplified system made of metal-dielectric composite in Cartesian coordinates. Given the subwavelength period of the nanolayers we assume validity of the effective medium theory (EMT), hence, for dielectric and metallic layers of the same thickness, the effective permittivities are manifested via the homogenization process $\varepsilon_x = 0.5(\varepsilon_d + \varepsilon_m)$, $\varepsilon_z = 2(\varepsilon_d^{-1} + \varepsilon_m^{-1})^{-1}$ [15], while the linear modes are plane waves. Each mode is characterized by its spatial frequency k_x, where the phase it acquires during propagation is determined by its propagation constant $k_z=(\varepsilon_x k_0^2-\varepsilon_x/\varepsilon_z k_x^2)^{1/2}$, this relation indicates that perfect imaging occurs when $\varepsilon_x=0$, where $\varepsilon_x > 0$ results in diffraction that will blur the image.

The system under investigation consists of metal-dielectric multilayers where the permittivity of the dielectric layers is assumed constant of $\varepsilon_d=3.2$. The close-to-resonance case is investigated at wavelength of $\lambda = 385$ with metal permittivity of $\varepsilon_m=-3.1-0.28i$ [16], while the off resonance propagation is studied at $\lambda = 365$ nm with $\varepsilon_m=-2.4-0.24i$. The k_z-k_x relations, which characterize the diffraction in the medium, are displayed in figure 1a.

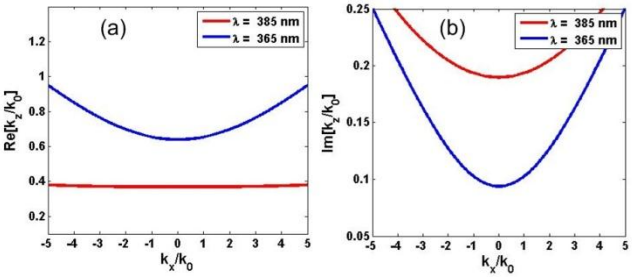

Fig. 1. Dispersion relation: Real (a) and Imaginary (b) parts of the propagation constant at $\lambda = 385$ nm (red) and $\lambda = 365$ nm (blue). Close to resonance (red lines) the dispersion is flat, indicating diffractionless propagation. However, the losses, corresponding to the imaginary part of kz are high. farther from resonance (blue), the dispersion is curved hence diffraction emerges. On the other hand, losses are decreased.

Close to the SPP resonance, the curve becomes flat owing to the fact that ε_x approaches zero. This indicates that the diffraction is arrested as all the plane wave

constituents acquire similar phase during propagation. Farther from resonance, the curve attains the hyperbolic shape, distinctive to indefinite media [7], resulting in anomalous diffraction characteristics [17,18]. The propagation losses, associated with the absorption due to ohmic losses in the metal, can be obtained from the imaginary part of k_z, shown in figure 1b. Close to resonance, one encounters much higher loss at a broad range of wavevectors. This example demonstrates the inherent trade-off between diffraction and loss in hyperbolic layered medium. This is evident from the linear propagation simulation shown in figure 2a,b, where the propagation of a sub-wavelength object, consists of two 40 nm slits separated by 90 nm is simulated through a 500nm thick hyperbolic medium, similar to that analyzed in figure 1. Indeed, the propagation at $\lambda = 385$ nm suffers high loss in the SPP resonance regime and shows a propagation distance of 1.5λ (Fig.2 – (a), red line in fig 2d). At the same time, a similar wavepacket at 365nm wavelength suffers lower loss but experience strong diffraction that smears the 2-slit object (Fig.2 – (b), green line in 2d), figure 2c depicts the nonlinear propagation where the dielectric layers possess Kerr nonlinearity. At Maximum index change of $\Delta n=0.035 \Delta n = 0.035$ the diffraction is arrested and the two-slits image is retained at the output, displaying higher efficiency (lower attenuation) compared with the linear resonant imaging.

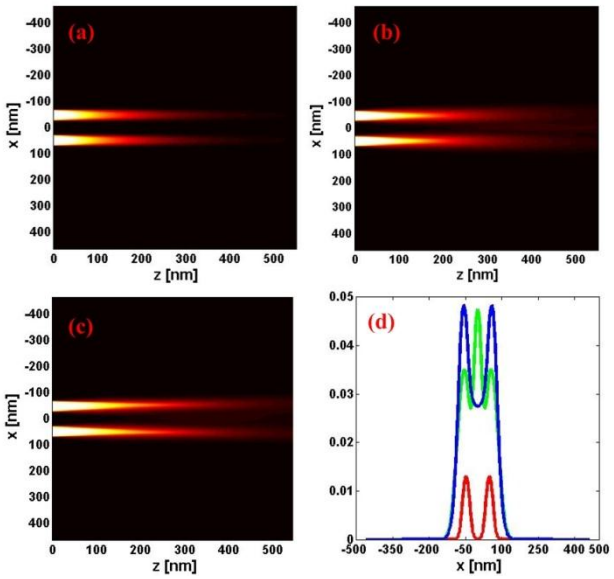

Fig. 2 Imaging of 2 Super-Gaussian sources 90 nm apart (a) Linear propagation close to resonance at λ = 385 [nm]. (b) Linear propagation far from resonance at λ = 365 [nm]. (c) Nonlinear propagation at λ = 365 [nm]. (d) Output intensities: close to resonance (red) the image is resolved but suffers high loss; far from resonance (green) the image is smeared due to strong diffraction; the nonlinear propagation in the medium (green) resolves the image with better efficiency.

The simulation is performed using noninear nonparaxial split-step Fourier beam propagation method (BPM) where the standard code has been modified so as to combine the electric and magnetic fields to one generalized electromagnetic field vector, yielding a first order partial differential equation [14,19]:

$$\frac{\partial}{\partial z}\Psi(x,z) = -iM_T(x)\Psi(x,z) \quad , \quad \Psi = \begin{pmatrix} H_z \\ E_x \end{pmatrix}$$

Where

$$M_T = \begin{pmatrix} 0 & k_0\varepsilon_x \\ k_0 - \frac{1}{k_0}\frac{\partial}{\partial x}\left(\frac{1}{\varepsilon_z}\frac{\partial}{\partial x}\right) & 0 \end{pmatrix}$$

The evolution of the electro-magnetic field over a small step Δz is therefore calculated by

$$\Psi(x,y,z+\Delta z) = e^{-iM_{NL}\Delta z} D_{\Delta z}\{\Psi(x,z)\} + O\left[(\Delta z)^3\right]$$

$D_{\Delta z}$ is the linear propagation operator defined as:

$$\Psi(x,z+\Delta z) = D_{\Delta z}\{\Psi(x,z)\} = \sum_{k_x} C(k_x, z_0) e^{ik_z(k_x)\Delta z}$$

Where $C(k_x,z_0)$ is the field projection on the linear mode $\exp(ik_x x)$ at $z = z_0$ which is the Fourier transform of the field. Each Fourier component acquires phase with its respective propagation constant. The nonlinear operator takes into account the permittivity modification via the Kerr-type nonlinearity, with the nonlinear polarization being

$$\overrightarrow{P_{NL}} = \frac{1}{2}\varepsilon_0\chi^{(3)}\left[|E|^2\vec{E} + \frac{1}{2}\left(\vec{E}\cdot\vec{E}\right)\vec{E}^*\right] = \varepsilon_x^{(NL)}E_x\hat{x} + \varepsilon_z^{(NL)}E_z\hat{z}$$

The nonlinear operator M_{NL} is calculated numerically as difference between M_T and M_L when M_T contains the nonlinear permativity $\varepsilon=\varepsilon_L+\varepsilon_{NL}$ while M_L is the same matrix with no nonlinearity - $\varepsilon=\varepsilon_L$. This method overcomes the problem of the linear and nonlinear operators not being separable in non-paraxial BPM.

Notwithstanding the importance of imaging through hyperbolic medium made of flat metal-dielectric layers, the effect of nonlinearity on super-resolution imaging is more pronounced in systems that are capable of delivering the sub-wavelength information to the far-field, such as optical Hyperlens. Investigating nonlinear super-resolution imaging in cylindrical hyperlens requires re-development of the BPM in cylindrical coordinates system where the propagation is in the *radial* direction. In what follows, we describe the first, to our knowledge, such cylindrical NL-BPM. The EMT for the same materials parameters as shown above but in cylindrical coordinates results in uniaxial medium with effective permittivities: ε_ρ, which is negative and ε_ϕ which is positive. The linear TM modes of such cylindrical Hyperbolic anisotropic medium are the complex order modified bessel functions (also termed Hyperbolic Bessel functions):

$$\Phi_m(\rho,\phi) = \left[J_{im\sqrt{\frac{\varepsilon_\phi}{|\varepsilon_\rho|}}}\left(k_0\sqrt{\varepsilon_\phi}\rho\right) + iY_{im\sqrt{\frac{\varepsilon_\phi}{|\varepsilon_\rho|}}}\left(k_0\sqrt{\varepsilon_\phi}\rho\right)\right] e^{im\phi}$$

These modes can penetrate to radii smaller than the wavelength even at high orders, unlike their conventiaonal counterparts, hence form the basis for the hyperlens operation [1]. Using the modified Bessel function, we derive similar formulation of Maxwell eqations, described by a first order PDE in Cylindrical coordinates:

$$\frac{\partial}{\partial\rho}\Psi(\rho,\phi) = -iM_T^{(Cyl)}\Psi(\rho,\phi) \quad , \quad \Psi = \begin{pmatrix} H_z \\ E_\phi \end{pmatrix}$$

Where

$$M_T^{(Cyl)} = \begin{pmatrix} 0 & -i\varepsilon_\phi k_0 \\ -ik_0 - \dfrac{i}{\rho^2\varepsilon_\rho k_0}\dfrac{\partial^2}{\partial\phi^2} & -\dfrac{1}{\rho} \end{pmatrix}$$

The linear propagation is now calculated by projecting the electro-magnetic field on the aforementioned modified bessel functions, contrary to plane waves as in Cartesian coordinates . the linear evolution of the field from radius ρ_0 to $\rho_0+\Delta\rho$ is calculated by :

$$\Psi(\rho_0+\Delta\rho) = D_{\Delta\rho}\{\Psi(\rho_0)\} = \sum_m A_m(\rho_0)\cdot\Phi_m(\rho=\rho_0+\Delta\rho,\phi)$$

Where $A_m(\rho_0)$ is the field projection on the m^{th} Hyperbolic bessel at $\rho=\rho_0$. The nonlinear operator is calculated in the same manner as in cartisian coordinates, as the difference between M_T and M_L .To the best of our knowledege this is the first NL-BPM in cylindrical coordinates which is capable of simulating propagation in the radial direction.

We utilize this radial BPM to simulate an input field comprised of two 40 nm FWHM gaussian beams with 75 nm seperation. The input radius is r_{in}=250 nm and output radius is r_{out}=1000 nm, indicating a 4-fold magnification at the hyperlens output. The hyperlens is made of dielectric layers with dielectric constant of ε_d =*3.2* and silver layers. We examine again two operation wavelengths: close to the Plasmon resonance frequency, at $\lambda = 385$ nm the metal permittivity is ε_m=*-3.1-0.28i*, while farther from resonance at $\lambda = 360$ nm, ε_m=*-2.2-0.23i*. Fig 3.(a) shows the propagation simulation of the sub-wavelength object close to the Plasmon resonance. Just like its Cartesian counterpart, the loss in the metal layers reduces the power significantly such that the signal is almost undetectable at the output. Moving away from the resonance at 360nm wavelength shows reduced loss but strong diffraction that smears the object (Fig 3b,3d-green). When incoporating the kerr nonlinearity, with a maximal refractive index change of $\Delta n = 0.013$at this wavelength, the diffraction is surpressed and the output is again resolved with 50X better efficiency (Fig.2c,2d – blue) and with 300nm separation which can be resolved with conventional diffraction-limited optics. Note that the diffraction arrest can be achieved with smaller nonlinear index change than in cartesian system; this is due to the different diffraction mechanism that dominates Hyperbolic Bessel functions compared with Plane waves.

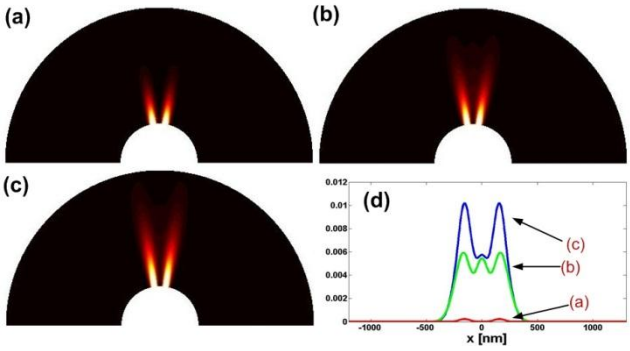

Fig. 3 Imaging of 2 Gaussian sources 75 nm apart in a Hyperlens with inner and outer radii of 240nm and 1000nm, respectively. (a)-(d) similar to figure 2.

In conclusion, we have shown that by incorporating self-defocusing Kerr nonlinearity in the dielectric constituents of hyperbolic Metamaterial one can suppress diffraction and achieve broad band operation and longer propagation distances. The longer propagation distance enables larger devices hence improves the spatial resolution: a 75nm separation at 360nm wavelength was demonstrated at moderate nonlinearity. Future reaserch may take into consideration the non local effects of the EMT [20], and an indepth investigation on the applicativity of the EMT in the Hyperlens configuration.

References

1. Z. Jacob, L. Alekseyev, and E. Narimanov, Opt. Exp. **14**, 8247–8256 (2006).
2. A. Salandrino and N. Engheta, PRB **74**, (2006).
3. Z. Liu, H. Lee, Y. Xiong, C. Sun, and X. Zhang, Science (New York, N.Y.) **315**, 1686 (2007).
4. I. I. Smolyaninov, Y.-J. Hung, and C. C. Davis, Science (New York, N.Y.) **315**, 1699–701 (2007).
5. J. Rho, Z. Ye, Y. Xiong, X. Yin, Z. Liu, H. Choi, G. Bartal, and X. Zhang, Nature communications **1**, 143 (2010).
6. E. Abbe, Archiv für mikroskopische Anatomie (1873).
7. D. Smith and D. Schurig, Phys. Rev. Lett. 1–5 (2003).
8. M. Scalora, G. D'Aguanno, N. Mattiucci, M. J. Bloemer, D. de Ceglia, M. Centini, A. Mandatori, C. Sibilia, N. Akozbek, M. G. Cappeddu, M. Fowler, and J. W. Haus, Optics Express **15**, 508 (2007).
9. A. J. Hoffman, L. Alekseyev, S. S. Howard, K. J. Franz, D. Wasserman, V. a Podolskiy, E. E. Narimanov, D. L. Sivco, and C. Gmachl, Nature materials **6**, 946–50 (2007).
10. J. Yao, Z. Liu, Y. Liu, Y. Wang, C. Sun, G. Bartal, A. M. Stacy, and X. Zhang, Science **321**, 930 (2008).
11. P. Belov and Y. Hao, Physical Review B **73**, 1–4 (2006).
12. J. Schilling, Physical Review E 1–8 (2006).
13. B. Wood, J. Pendry, and D. Tsai, Phys. Rev. B **1**, 1 (2006).
14. Y. Liu, G. Bartal, D. Genov, and X. Zhang, Physical review letters **153901**, 1–4 (2007).
15. D. Bergman, Physics Reports **9**, 377–407 (1978).
16. P. Johnson and R. Christy, Phys. Rev. B **1318**, (1972).
17. R. Morandotti, H. Eisenberg, Y. Silberberg, M. Sorel, and J. Aitchison, Phys. Rev. Lett. **86**, 3296 (2001).
18. T. Pertsch, T. Zentgraf, U. Peschel, a. Bräuer, and F. Lederer, Physical Review Letters **88**, 4–7 (2002).
19. A. Sharma and A. Agrawal, JOSA A **21**, 1082 (2004).
20. J. Elser, V. A. Podolskiy, I. Salakhutdinov, and I. Avrutsky, Applied Physics Letters **90**, (2007).